THE JOURNAL OF PHYSICAL CHEMISTRY C

Article

pubs.acs.org/JPCC

High-Resolution Quantum Dot Photopatterning via Interference Lithography Assisted Microstamping

Sidney T. Malak,[†] Guanquan Liang,[‡] Ramathasan Thevamaran,[‡] Young Jun Yoon,[†] Marcus J. Smith,[†,§] Jaehan Jung,[†,∥] Chun Hao Lin,[†] Zhiqun Lin,[†] Edwin L. Thomas,[‡] and Vladimir V. Tsukruk*[,†]

[†]School of Materials Science and Engineering, Georgia Institute of Technology, Atlanta, Georgia 30332, United States

[‡]Department of Materials Science and NanoEngineering, Rice University, Houston, Texas 77005, United States

[§]Aerospace Systems Directorate, Air Force Research Laboratory, Wright-Patterson Air Force Base, Dayton, Ohio 45433, United States

[∥]Department of Materials Science and Engineering, Hongik University, Sejong 339-701, South Korea

Supporting Information

ABSTRACT: We present novel photopatterning approaches based on near-field and far-field interference lithography techniques that yield highly uniform high-resolution large-area face-profile and edge-profile photopatterns. The near-field interference methods utilize a phase-shift mask while the far-field method uses two-beam interference. These interference-based techniques yield photopatterns with minimum feature sizes near 500 nm, which matches the current resolution of photopatterning. Furthermore, these interference techniques drastically increase the patternable area (up to cm^2) and the throughput (increases of up to 3 orders of magnitude) while maintaining pattern uniformity. Furthermore, these strategies use easy-to-handle reusable photomasks or no masks at all and address the major constraints associated with obtaining high resolution without compromising throughput that have often limited the applicability of traditional photopatterning. Finally, all approaches can be applied multiple times on the same film area to yield ultradense multilevel intensity contrast photopatterns that are very difficult to obtain using traditional strategies. These interference-based exposure techniques represent a paradigm shift in the field of photopatterning and will be valuable for applications that require uniform high-resolution patterns over large areas, such as photosensors, anticounterfeiting labels, and virtual displays.

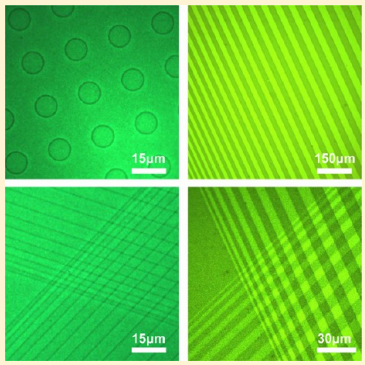

INTRODUCTION

The field of photonics has experienced a variety of recent achievements, including broader spectral range lasers, more efficient light-emitting diodes (LEDs), and improved light harvesting energy systems.[1−4] Many of the developments have been driven by advances in the area of microscale and nanoscale patterning techniques.[5−7] There are a wide variety of micro/nanoscale patterning techniques and designations. One of the most important distinctions is whether the patterning technique is a serial or parallel process.[8,9] A serial process fabricates one structure at a time via a direct-write approach (e.g., electron beam lithography (EBL) or focused ion beam milling (FIB)). These techniques often have high resolution (below 50 nm) but low throughput.[8,9] In contrast, a parallel process fabricates multiple structures simultaneously and includes processes like photolithography, colloidal lithography, and soft-lithography.[10,11] The throughput of these techniques is typically high but sometimes have a trade-off in resolution.[10,12] Another important patterning classification is whether the technique yields physical or nonphysical patterns. Physical patterning involves the addition, removal, and/or rearrangement of material to create a pattern and includes most of the techniques listed above.[8,9] Nonphysical patterns are those that involve the intrinsic modification of the material properties to provide contrasts in the chemical nature, ion doping concentration, stiffness, or photoluminescence emission intensity, and which do not have an extrinsic physical pattern.[13−16] For example, photoluminescence (PL) photopatterns can be fabricated using unstable light-sensitive quantum dots (QDs) that exhibit variations in intensity or undergo spectral shifts when exposed to light.[13,14,16] QDs are ideal candidates for photopatterns due to their size-dependent emission across the visible spectrum, high quantum yield, narrowband emission, and compatibility with surface functionalization techniques.[17−22] The combination of characteristics exhibited by photopatterns and quantum dots allows for potential applications in anticounterfeiting, light sensing, and display technologies.[14,15]

A variety of studies have outlined photopatterning strategies that yield photopatterns with high intensity contrast and single (or multiple) colors.[14,15,23] Furthermore, photopatterns can be stored for a long period of time and then recharged using light

Received: April 20, 2017
Revised: May 30, 2017
Published: May 30, 2017

DOI: 10.1021/acs.jpcc.7b03731
J. Phys. Chem. C 2017, 121, 13370−13380

exposure, which quickly and effectively reverses much of the pattern fading that occurs over time.[14] Development in the field of photopatterning has been driven in part by inexpensive and widely available photomasks (often Cu TEM grids).[13−15,24] Although initial results are promising, a number of important limitations remain in terms of poor resolution (feature sizes are generally tens of microns or more) and low throughput (small areas and long development times). Some studies have attempted to bridge the resolution gap by employing TEM grids with smaller feature sizes (∼7 μm).[15] However, this does not address the fundamental limitations associated with binary transmission-based photomasks. Photopatterning has been demonstrated using a scanning laser-based exposure setup. This significantly improves resolution (feature size of ∼575 nm) but is a serial process with low throughput.[23] Clearly new photomasks and exposure strategies need to be identified that can address the obstacles associated with resolution and throughput.

A number of patterning approaches exist that could overcome the current limitations in resolution and throughput of photopatterning. These techniques use either near-field or far-field light interference to obtain very small feature sizes, and moreover, work via a parallel process that allows for high throughput. Near-field phase-shift lithography is a particularly promising interference technique because it is a parallel process that can pattern features down to 90 nm.[25] This approach uses a robust patterned PDMS stamp to obtain specific predetermined regions of destructive interference.[25−27] Additionally, patterned PDMS stamps can be fabricated with arbitrary shapes.[10] Far-field interference patterning via laser interference lithography (LIL) can also create high-resolution patterns over large areas.[28,29] LIL uses two or more coherent light beams to create an interference pattern and has been shown to be an efficient method for fabricating micron to submicron scale structures for photonic, phononic, and structural applications.[28,29] A variety of patterns can be generated by LIL depending on the number of interfering beams and exposure steps. For example, 1D gratings with very uniform periodicity can be fabricated by utilizing the traditional multibeam one-step exposure approach.[28] Higher dimensional patterns (cross-hatched, diamond symmetry structures) can also be developed using dual-beam multiple-step exposures or an elliptical polarization triple beam setup.[30−32] Traditionally, near-field and far-field interference approaches have been implemented to initiate cross-linking or chain scission reactions in polymer films to create physical patterns.[25−27,29,30]

In this work, we outline novel photopatterning strategies based on interference-lithography that yield high resolution photopatterns in QD-polymer composites. The near-field interference approaches employ patterned PDMS stamps and specific exposure conditions to create unique edge-profile or face-profile photopatterns. The far-field interference approach utilizes a two-beam laser interference lithography setup to produce a photopattern with sinusoidal intensity modulation. The capabilities of these approaches stem from their being based on near-field and far-field interference phenomena, which represents the first use of these exposure phenomena in the field of photopatterning. These approaches yield high-throughput large-scale highly uniform photopatterns with predetermined designs and overcome many of the issues associated with serial laser scanning exposure and photopatterning approaches that use traditional photomasks.

EXPERIMENTAL METHODS

Chemicals and Materials. Cadmium oxide (CdO), tri-*n*-octylphosphine (TOP, 90%), tributylphosphine (TBP, >93.5%) and poly(methyl methacrylate) (PMMA; M_W = 120000) were obtained from Sigma-Aldrich. Selenium powder (Se, 99.999%), 1-tetradecylphosphonic acid (TDPA, 98%), tri-*n*-octylphosphine oxide (TOPO, 90%), diethylzinc (15 wt% in hexane), and hexane were obtained from Alfa Aesar. Hexadecylamine (HDA, 90%) and bis(trimethylsilyl) sulfide (95%) were obtained from TCI. Toluene was obtained from BDH Chemicals. All chemicals were used as received.

Synthesis of Unstable Yellow and Green CdSe/ZnS QDs. Green and yellow emitting CdSe QDs were synthesized following a literature procedure.[15,33] First, 50 mg of CdO, 300 mg of TDPA, and 4 g of TOPO were injected into a three neck flask. The mixture was heated to 120 °C and degassed for 1 h. Next, the temperature was increased to 290 °C under Argon. After the solution became clear, 1 mL of 1 M Se/TBP solution was quickly injected to initiate nucleation and growth. Green CdSe QDs were grown at 290 °C for 10 s while yellow CdSe QDs were grown for 30 s. Following this growth, the heating mantle was removed to stop the reaction. Once the temperature fell to 70 °C, 5 mL of hexane was added to the solution.

The ZnS shell of the unstable (green and yellow) CdSe/ZnS core/shell QDs was synthesized following a reported procedure.[34] Briefly, 2 g of TOPO and 1 g of hexadecylamine (HDA) were injected into a three-neck flask and degassed at 120 °C for 1 h. After this, 5 mL of CdSe core QDs was added and the temperature was increased to 220 °C under argon. Precursor solution (0.15 mL of diethylzinc and 0.05 mL of bis(trimethylsilyl) sulfide in 1 mL of tri-*n*-octylphosphine) was then injected dropwise to the (vigorously stirring) reaction mixture. The reaction was allowed to proceed for 30 min to grow the ZnS shell. Following this growth, the heating mantle was removed to stop reaction. Five ml of hexane was added to the solution when the temperature fell to 70 °C. The green and yellow CdSe/ZnS QDs had PL emission of ∼528 and ∼592 nm, respectively.

Sample Preparation. QD-polymer films had thickness ranging from 260 ± 50 to 560 ± 60 nm (as evaluated by ellipsometry) depending on spin conditions and polymer solution concentration. Films were prepared by spin-casting a QD-polymer mixture at 2000−2500 rpm for 1−1.5 min, as outlined in a previous publication.[14,15] Films typically had a QD-loading near or below 1% (volume fraction), which was estimated by ellipsometry (Bruggeman model).[35] The QD-polymer mixture was composed of equal parts of a QD toluene solution and a 10−12% PMMA toluene solution, and vortexed to ensure complete mixing. Films were deposited on silicon with a 290−295 nm surface layer of SiO_2. The QD-polymer films were typically covered or placed in dark environments immediately after spin-casting to minimize exposure from ambient light before the photopatterning process.

Electromagnetic Simulations. COMSOL Multiphysics (v5.1) was used to perform electromagnetic simulations of the near-field destructive interference phenomenon. The light intensity distribution was simulated for UV and blue light passing through a model that closely matched the real PDMS stamp and QD-polymer film system. Periodic boundary conditions were applied in the case where a single period was examined. The pattern on the PDMS mask matched the real

DOI: 10.1021/acs.jpcc.7b03731
J. Phys. Chem. C 2017, 121, 13370−13380

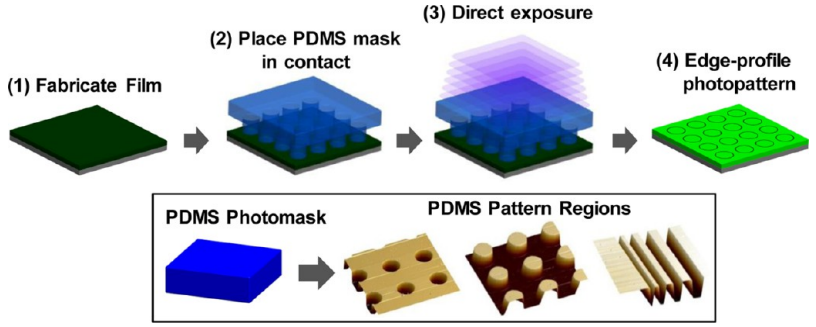

Figure 1. "Direct exposure" photopatterning process using a PDMS stamp. (1) QD-polymer film is deposited and (2) a PDMS stamp is placed on its surface. (3) Light is incident on the patterned region of the PDMS stamp (direct exposure incidence). (4) When the PDMS stamp is removed, a photopattern is present corresponding to the edge-profile of the PDMS pattern. (Bottom panel) 3D AFM images of the patterned regions of the various PDMS photomasks used in this study.

system characteristics (1.1 um thick, 20 um period, 1.42 refractive index). The air void regions also matched the real system (thickness of 1.1 um and refractive index of 1.00). The QD-polymer film had a thickness of 550 nm and refractive index of 1.5. The substrate under the QD-polymer film was silicon (refractive index of 4.04) with a surface layer of SiO_2 (thickness of 292 nm and refractive index of 1.46). Reflected and transmitted light is absorbed by the perfect match layers (PMLs) placed at the top and bottom of the system. A single wavelength light source is set at the bottom edge of the top PML. The center wavelength of the UV filter (350 nm) and blue filter (470 nm) were used to approximate the bandpass spectrum.

Photomask and Photopattern Development. The patterned polydimethylsiloxane (PDMS) photomasks (used for near-field photopatterning) were fabricated using a common fabrication procedure for PDMS soft-lithography stamps.[10,27] PDMS patterns of various size, shape, and spacing were dictated by a chrome master pattern on a quartz substrate. The height of the patterned features on the PDMS photomask were 1.1−1.2 μm. Photopatterning using the near-field patterned PDMS stamp used a 10× objective (NA: 0.30) with either UV (325−375 nm) or blue (450−490 nm) light over a range of powers, as outlined in previous work.[14,15] The light source was a 120 W Hg vapor short arc lamp (X-cite series, 120Q, Lumen Dynamics) with controllable power output. To ensure consistent light exposure, the light source was typically focused on the top surface of the PDMS stamp during the photopattern development.

Far-field photopatterning via laser interference lithography was conducted by creating an interference pattern using two interfering laser beams.[28,30,31] Specifically, a 532 nm laser beam was output from a Coherent Verdi 5 system and then passed through a beam splitter cube to create two coherent laser beams. The two beams traveled the same optical path length after the beam-splitting point. Each beam was expanded to have a diameter of approximately 18 mm. The power density of each beam was measured to be near 955 mW/cm^2. The two beams were symmetrically incident on the same side of the polymer film at an incident angle "θ" with respect to the normal of the film. An angle of 3.05° was used to obtain a sinusoidal periodicity "a" of approximately 5 μm (predicted via $a = \lambda/2 \sin \theta$). A high interference contrast of the two beams was obtained by utilizing parallel linear polarization. The interference pattern manifested itself as a 1D grating on the polymer-quantum dot film. The cross-hatched array was fabricated using a two-step exposure of the 1D grating by mounting the QD-polymer film on a rotational stage and rotating 90° after the first exposure for the consequent exposure. Short light exposure times were used to minimize the effects of spatial drift on the photopattern contrast.

Characterization. Characterization of the photopatterns outlined in this work followed procedures outlined in previous works.[14,15] Briefly, photoluminescence spectroscopy of the QD-polymer films was performed using a CytoViva Hyperspectral scanning system with a diffraction grating spectrophotometer (spectral range of 400−1000 nm, spectral resolution near 2.8 nm). Optical microscopy (bright field, dark field, and photoluminescence) images of the QD-polymer films and photopatterns were collected using a cooled Dagexcel-M Digital Firewire camera. Objectives of 10× (NA: 0.30), 50× (NA: 0.8), and 100× (NA: 0.9) magnification were employed. The photoluminescence filter setup was the same as employed in a previous work.[15] The light source was the 120 W Hg vapor short arc lamp, X-cite series, 120Q, Lumen Dynamics. The power and intensity values for the UV (325−375 nm) and blue (450−490 nm) light exposure represent the power and intensity at the approximate peak wavelength of each range (350 and 470 nm, respectively). The PL cross sections of a photopattern were obtained using the "plot profile" capability of ImageJ (1.48v), where the size of the image was specified by inputting known pixel/μm scaling from the Dagexcel-M Digital Firewire camera.[14] The thickness of the QD-polymer films was measured using a spectroscopic ellipsometer (Woollam, model M2000) in accordance with previously outlined procedures.[14,15] AFM scans (topographical and phase) were collected with on Dimension Icon AFM microscope (Bruker) in tapping mode (MikroMasch tips).[36] Scans commonly had a size of 60 μm by 60 μm with a scan rate within 0.3−0.8 Hz.

RESULTS AND DISCUSSION

In this section, we will first discuss different approaches for photopatterning and then will compare these approaches.

Photopatterning via Direct Exposure (PDMS Mask). Photopatterns were fabricated by selective light exposure to a light sensitive film, as outlined in previous works.[14,15] In this case, the light-sensitive film is a CdSe/ZnS QD-polymer composite that exhibits an increase in its QD PL intensity when exposed to light over many minutes (Supporting Information, Figure S1a). The QDs have photoluminescence emission in the green (~528 nm) and yellow (~592 nm) wavelength regions (Figure S1b). The core/shell quantum dots utilized in this

DOI: 10.1021/acs.jpcc.7b03731
J. Phys. Chem. C 2017, 121, 13370−13380

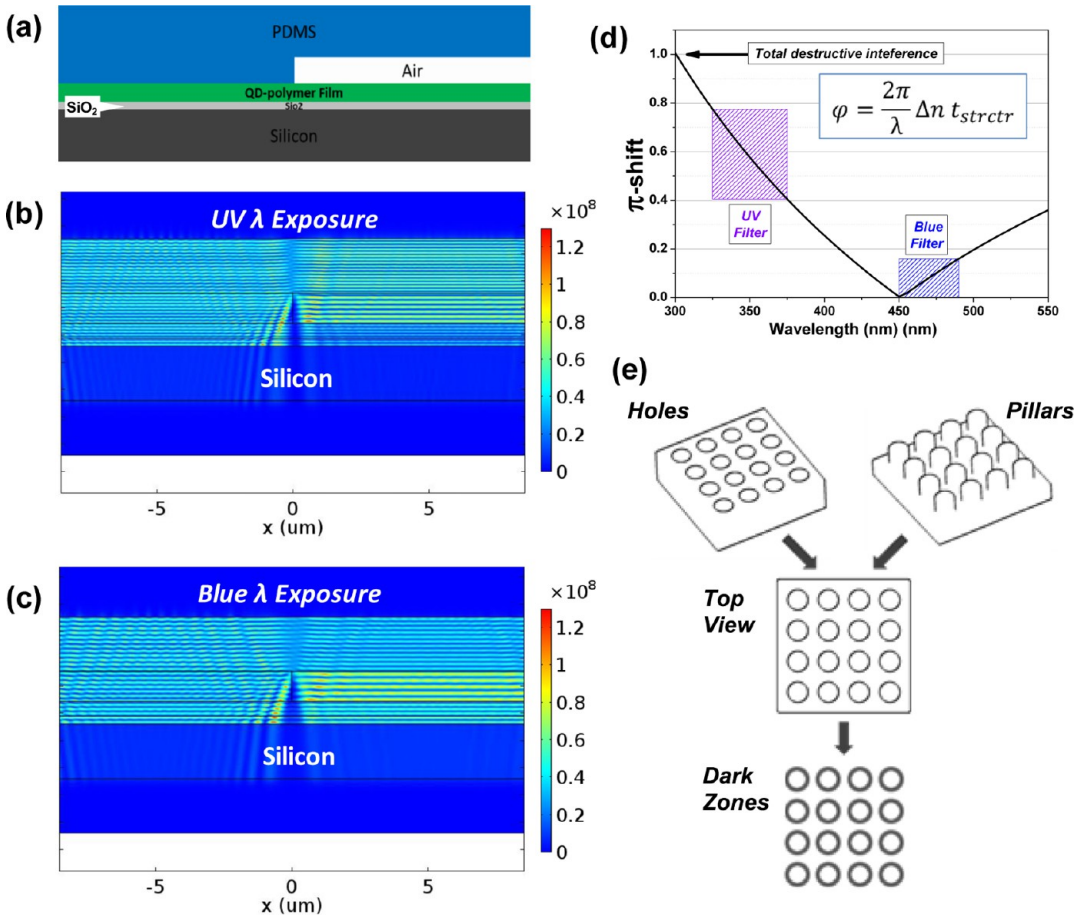

Figure 2. Electromagnetic simulations and theoretical expectations predict the near-field destructive interference phenomenon that underlies direct exposure photopatterning. (a) Schematic of the model used for electromagnetic simulations (one period of the array). (b, c) Simulated light intensity distribution within one period of the array for the UV and blue exposure, respectively. (d) Relationship between the phase shift (between light in the PDMS and in the air gaps of the PDMS pattern) and the wavelength of exposure light. (e) Schematic of "direct exposure" edge-profile photopatterning and its insensitivity to the *z*-profile of the PDMS stamp (pillar vs hole) since the lateral cross-section is the same in both cases.

study display a change of PL intensity when exposed to light due to photooxidation and photobleaching. Briefly, decay and enhancement of QD PL intensity upon exposure to ambient environments and high intensity visible light occurs due to degradation of the QD shell and modification of the QD core. The spectral blue shifting during this process suggests photo-oxidation and corrosion are likely occurring at the QD shell, core/shell interface, and eventually core surface.[13,14,16]

The photopatterning process begins by depositing a QD-polymer film onto a substrate (Figure 1, step 1) and then a polydimethylsiloxane (PDMS) stamp with a patterned surface is brought into conformal contact with the film (Figure 1, step 2). The system is then exposed to light of a wavelength that the QDs can absorb (Figure 1, step 3). It is critical to mention that the exposure light is directly incident on the patterned region of the PDMS mask (termed "direct exposure").

direct exposure pattern → light beam directly incident on patterned mask region

edge-profile pattern → photopattern mimics edges of mask pattern

(ex. circular mask structure → ring photopattern)

The PDMS photomask modulates the exposure light in certain regions while leaving the light intensity in other regions unchanged. The spatially modulated light intensity is incident on the underlying light-sensitive QD-polymer film, leading to a contrast in the amount of PL recovery that occurs in different regions. For example, high exposure regions undergo significant PL recovery while low exposure regions do not. After the PDMS mask is removed, a photopattern can be observed (Figure 1, step 4). A unique characteristic of direct exposure PDMS photopatterning is that the resulting photopatterns are defined primarily by the edges of the PDMS pattern (discussed in detail later). For example, a circular hole or a circular pillar in the PDMS mask will both yield a dark circular ring photopattern (Figure 1, step 4).

The unique "edge-profile" photopattern results from the distinct near-field phase-shift interference phenomenon that occurs within the PDMS pattern.[25−27] It is important to note that this phase-shift approach is in stark contrast to photo-patterning that uses a binary photomask composed of opaque materials like Cu (TEM grid) or Cr (photolithograph mask).[13−15,24,37] Metal masks provide light exposure contrast to the underlying light responsive film by blocking the passage of light through the binary photomask in certain regions via reflection or absorption. Therefore, areas of the light-responsive film protected by the photomask remain unchanged while areas

DOI: 10.1021/acs.jpcc.7b03731
J. Phys. Chem. C 2017, 121, 13370−13380

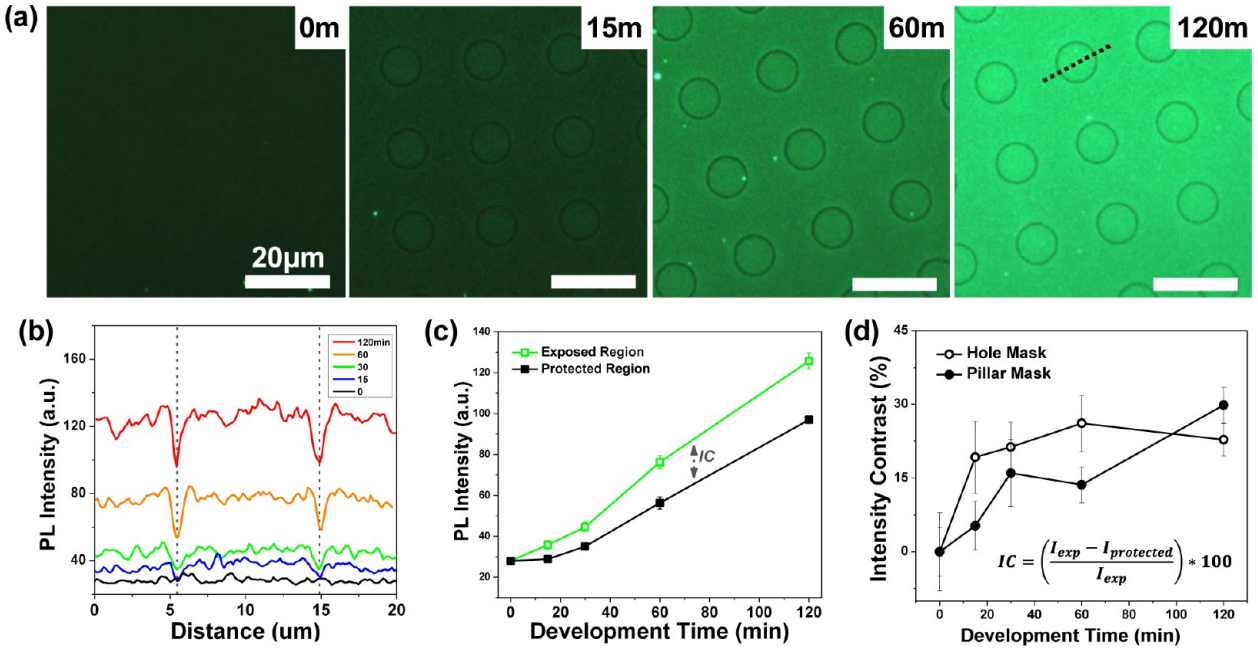

Figure 3. Demonstration of the "direct exposure" photopatterning process using a PDMS stamp with a hole array pattern. (a) PL images of a circular edge-profile photopattern at different stages of pattern development (developed using UV light (325−375 nm), 19.8 mW/cm^2). (b) PL intensity cross-section across edge-profile rings. (c) PL intensity of the protected and exposed regions of the photopattern, and (d) the intensity contrast (IC) at different stages of pattern development using a hole or pillar PDMS photomask. Scale bar is 20 μm for all images.

of the film exposed to the development light undergo a change of their PL (increase/decrease of intensity or spectral shift).[13,14]

However, a PDMS photomask is nearly transparent to the development light and therefore modulates light intensity using a fundamentally different mechanism than the opaque binary photomask.[25−27] In the case of a transparent photomask, modulation of light intensity arises from destructive/constructive interference at certain regions of the patterned interface of the PDMS photomask originating from a near-field phase-shift (NFPS).[25−27] Briefly, light that propagates through the patterned PDMS stamp will encounter various paths through either recessed (hole) or raised (pillar) microstructures and a second medium (typically air). The difference in refractive index between PDMS ($n_{PDMS} \approx 1.41$) and air ($n_{air} \approx 1.00$) can lead to a phase difference between light traveling in the PDMS and air at the vertical feature interface (Supporting Information, eq S1). If the phase difference is an odd multiple of π, then destructive interference occurs and the light intensity will be zero, which means no PL recovery occurs in this region of the light-responsive QD-polymer film.

Electromagnetic simulations of the light intensity within a single period of a PDMS patterned array show that UV (350 nm) and blue (470 nm) light both experience some degree of destructive interference at the vertical edge of the PDMS patterned surface, as noted by the dark blue region (Figure 2a−c). This phenomenon can also occur over many periods of a PDMS patterned array (Figure S2). Theoretical predictions also indicate that destructive interference for UV and blue wavelengths is expected in this system (Figure 2d). The phase shift is given by the equation in the Figure 2d, inset, with actual system parameters ($\Delta n = 0.41$, $t_{strctr} = 1.1$ μm, where t is the structure thickness).

Phase shift values closer to π indicate destructive interference (odd integer of π phase difference). The simulation and theory both predict that UV wavelengths will experience a greater degree of destructive interference than the blue wavelengths. Moreover, the destructive interference is a highly localized near-field phenomenon since it is arises from destructive interference of the evanescent waves at the PDMS−air interface, which means subwavelength features can be patterned.[25−27] Finally, since the near-field phase-shift destructive interference phenomenon occurs at the vertical edges of the PDMS structures, the shape and size of the PL photopattern should depend solely on the lateral projection of the PDMS pattern and should not be sensitive to whether the PDMS pattern is raised (pillars) or recessed (holes; Figure 2e).

To verify these predictions, we conducted direct exposure photopatterning using patterned PDMS photomasks of either circular hole or circular pillar arrays that have the same dimensions and arrangement (Figures S3 and S4). Photoluminescence images of a photopattern of circular rings, which was created using a patterned PDMS photomask of circular holes, proves that the photopattern is indeed of the edge-profile type (Figure 3a−d). The PL images also show that longer development times increase both the PL intensity and contrast of the photopattern (Figure 3a). PL cross sections of the PL images quantifiably confirm the increase of PL intensity with exposure time and make it possible to measure the PL intensity of the dark and bright regions of the pattern (Figure 3b,c). The intensity contrast, which is a measure of the difference of PL between dark and bright regions of a pattern, increases with development time (Figure 3d).

This approach and behavior is consistent with the PL recovery mentioned earlier and with previous studies (Figure S1).[14,15] Photopatterns result from intrinsic modification of the QDs within the QD-polymer film and are not due to physical addition, removal, or rearrangement of material from the film.[13−15,24,37] The featureless topography is confirmed by atomic force microscopy (AFM) scanning of the film in regions that have been photopatterned (Figure S5).

DOI: 10.1021/acs.jpcc.7b03731
J. Phys. Chem. C 2017, 121, 13370−13380

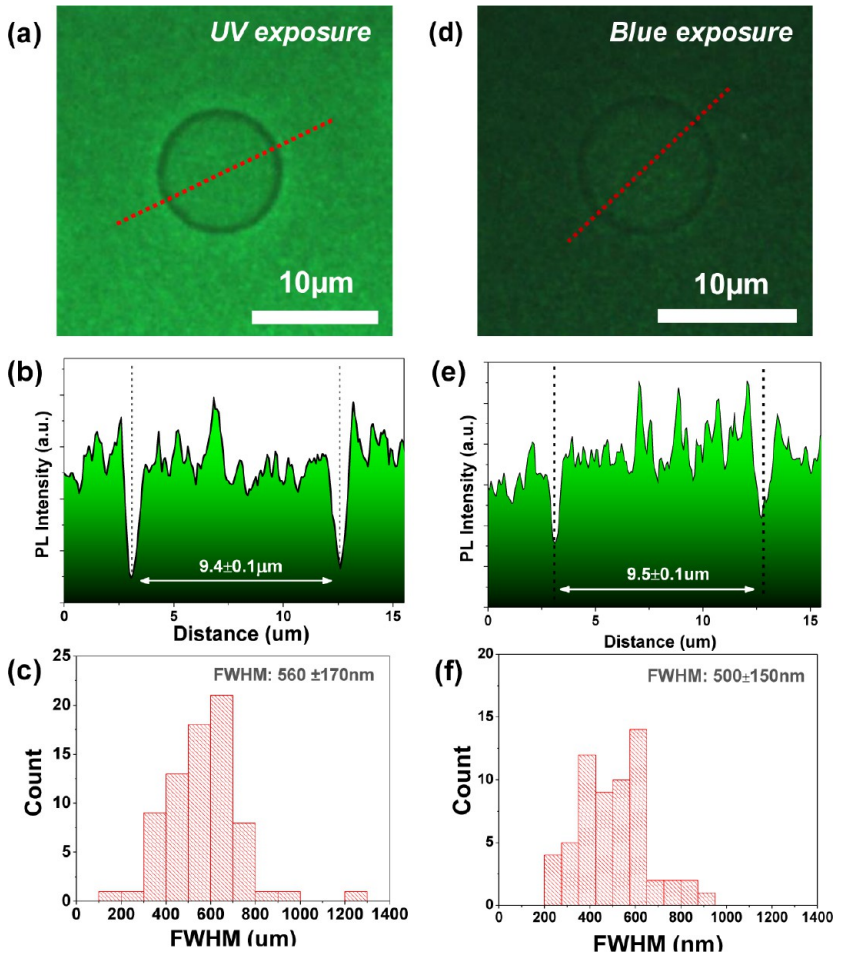

Figure 4. PL images, their intensity cross-section, and fwhm histogram of photopatterned rings made using the "direct exposure" approach with (a–c) UV (325–375 nm) and (d–f) blue (450–490 nm) development light (10 μm hole photomask).

The insensitivity of direct exposure photopatterning to the recessed/raised nature of the PDMS photomask was confirmed by fabricating a photopattern with a patterned PDMS photomask of raised circular pillars. PL imaging shows a photopattern that is practically identical to the photopattern created using a hole PDMS photomask (Figure S6), with the majority of the photopattern contrast occurring at the edges of the pattern of the PDMS photomask (in this case the circumference of each pillar or hole). In addition, the patterned hole and pillar PDMS photomasks yield photopatterns with similar intensity contrast (Figure 3d).

An important characteristic of the edge-profile photopattern is that it has feature sizes extending down to the submicron region (fitting of PL cross-section shows a full-width half-maximum ~500–560 nm), which was previously only possible using a scanning laser-based exposure setup (Figure 4).[23] The submicron feature size can be obtained using either UV (325–375 nm) or blue (450–490 nm) exposure light (Figure 4b–f) and a recessed hole or raised pillar PDMS photomask (Figures 4 and S7). However, the intensity contrast obtained from blue exposure (19%) is lower than that provided by UV exposure (24%) since blue wavelengths do not adhere as closely to the requirements for complete destructive interference (π-shift) as the UV wavelengths (Figure 2d; eq S1).[25]

For the PDMS mask used in this study, higher intensity contrasts could theoretically be obtained using wavelengths that more closely match the destructive interference requirement (for example, 902 nm). However, the decrease in absorbance of the green QDs past ~530 nm limits the exposure wavelengths that can be utilized. The observed full-width half-maximum (fwhm) of the edge-profile photopattern fabricated using UV and blue development light matches predictions from electromagnetic modeling (500–540 nm) shown in Figure S8b,c.

Furthermore, electromagnetic modeling shows that the fwhm of the destructive interference region increases deeper into the QD-polymer film (Figure S8b,d). In fact, a difference of 40 nm in fwhm between the top and bottom of the 550 nm thick QD-polymer film is predicted for the UV exposure case. The increase of fwhm with greater depth will degrade intensity contrast and lead to an apparent degradation of resolution. Ideally, the fwhm would be depth-independent so that the line resolution would be consistent between thin and thick QD-polymer films.

The edge-profile photopatterning is different from traditional photopatterns, which replicate the mask's pattern[13−15,24,37] because the primary intensity contrast of the edge-profile photopatterns stems from their edges. However, the edge-profile patterns do have some face-profile intensity contrast (increase of PL intensity in the internal regions), but this is only clearly evident at lower viewing magnifications (Figure S9).

Photopatterning via Indirect Exposure (PDMS Mask). Patterned PDMS stamps have a number of advantages over the traditional metal photomasks typically used in photopatterning

DOI: 10.1021/acs.jpcc.7b03731
J. Phys. Chem. C 2017, 121, 13370−13380

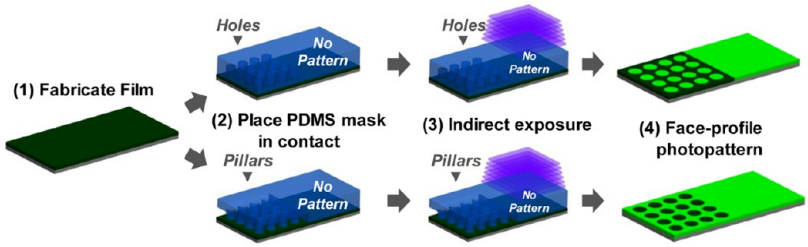

Figure 5. "Indirect exposure" photopatterning process using a PDMS stamp. (1) QD-polymer film is deposited and (2) a PDMS stamp is placed on its surface. (3) Light is incident on the PDMS stamp on a region where there is no underlying physical PDMS pattern (indirect exposure light incidence). (4) When the PDMS stamp is removed a positive photopattern is present corresponding to the face-profile of the regions of the PDMS patterns (so the pillar and hole patterns will yield different patterns). In this case the photopattern is due to indirect scattered and waveguided light that travels through the PDMS stamp to the patterned (hole and pillar) regions.

(e.g., TEM grids). These advantages include PDMS being more robust than TEM grids (allowing them to be reused), easier to handle (making patterning more simple and reliable), and having higher resolution and more pattern choices (permitting more applications). However, PDMS also has a very different complex refractive index than metals in the near UV and visible wavelength ranges (specifically, $n_{PDMS} \sim 1.4$ and $k_{PDMS} \sim 0$), which enables it to waveguide light with minimal optical attenuation losses. Optical waveguiding and scattering, in turn, makes possible a unique indirect exposure approach that is not possible using traditional metal photomasks. This unique exposure approach is termed the "indirect exposure" approach.

The specific steps of the indirect exposure approach are outlined in Figure 5. Overall, this approach is similar to the direct exposure approach outlined earlier except that indirect light incidence is used to develop the photopattern. In this scenario, the development light is incident on a region of the PDMS photomask that is not patterned (Figure 5, step 3).

When light enters the PDMS material, much of the light propagates to the underlying QD-polymer film due to the high optical transparency of PDMS from 250 to 1100 nm. However, light also diffuses/scatters in the lateral directions due to the presence of silica nanoparticles and other localized contaminants in the commercial PDMS material. The scattered light can propagate to the patterned surface of the PDMS mask to "indirectly expose" the underlying light-sensitive QD-polymer film, which then forms a photopattern.

There are a number of important differences between the indirect exposure approach and the direct exposure approach. First, indirect exposure patterning is based on waveguiding to localized scattering at the patterned PDMS structures and therefore does not require adherence to a strict relationship between the mask dimensions and exposure wavelength (as outlined by eq S1). Second, indirect exposure yields more traditional "face-profile" photopatterns (i.e., a circular PDMS pillar will yield a photopatterned circle; Figure 5, step 4). Finally, the resulting photopattern depends on whether the PDMS pattern is recessed or raised (because waveguiding and localized scattering develop the photopattern; Figure 5, step 4). The indirect exposure patterning approach is demonstrated using a PDMS stamp with either recessed circular holes or raised circular pillars (Figure 6a,b and c,d, respectively). PL imaging of these photopatterns reveals a number of important observations.

First, the indirect exposure approach yields face-profile photopatterns, as opposed to the edge-profile photopatterns shown earlier using the direct exposure approach. Second, the contrast of the photopattern increases with longer development

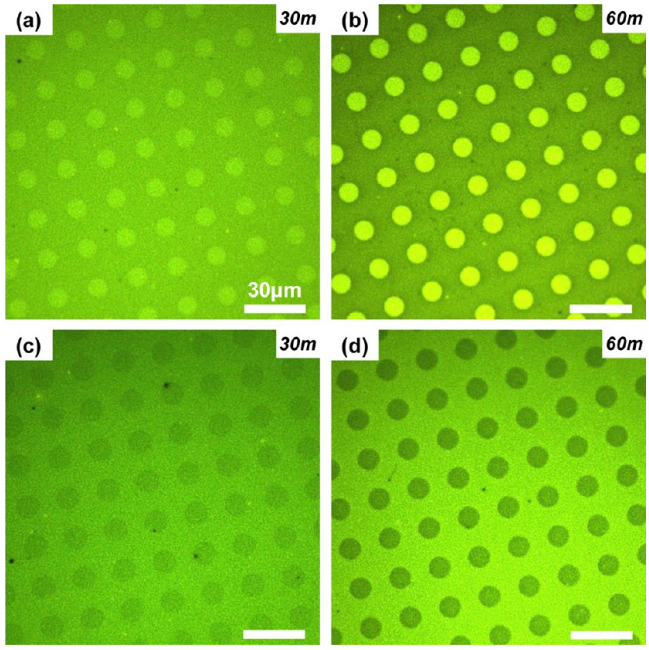

Figure 6. PL images of photopatterns developed using the indirect exposure approach. (a, b) PL image of a photopattern fabricated using a PDMS mask of 10 μm holes. (c, d) PL image of a photopattern fabricated using a PDMS mask of 10 μm pillars. Patterns were developed using UV light (325−375 nm; 15 mW/cm^2). Scale bar is 30 μm for all images.

time. And finally, the resulting photopattern strongly depends on whether the PDMS pattern was recessed or raised. A PDMS stamp with recessed circular holes yields high intensity circles, while a PDMS stamp with raised circular pillars yields low intensity circles (or a surrounding area of high intensity). The exact mechanisms underlying this trend are not clear because light from the PDMS photomask can enter the light-sensitive QD-polymer film via both optical scattering and waveguide bleeding. However, it is clear that the recessed holes cause light to enter the underlying QD-polymer film more efficiently than the raised pillars since PDMS holes lead to bright circular disks and QDs undergo an increase in PL intensity when exposed to light (Figure S1a). The positive and negative face-profile photopatterns (resulting from PDMS hole and pillar photomasks, respectively) are present over larger lateral areas as well (mm^2; Figure S10). These demonstrations clearly show that very different types of photopatterns can be obtained by simply changing how the exposure light is incident on the patterned PDMS photomask (direct exposure vs indirect exposure).

DOI: 10.1021/acs.jpcc.7b03731
J. Phys. Chem. C 2017, 121, 13370−13380

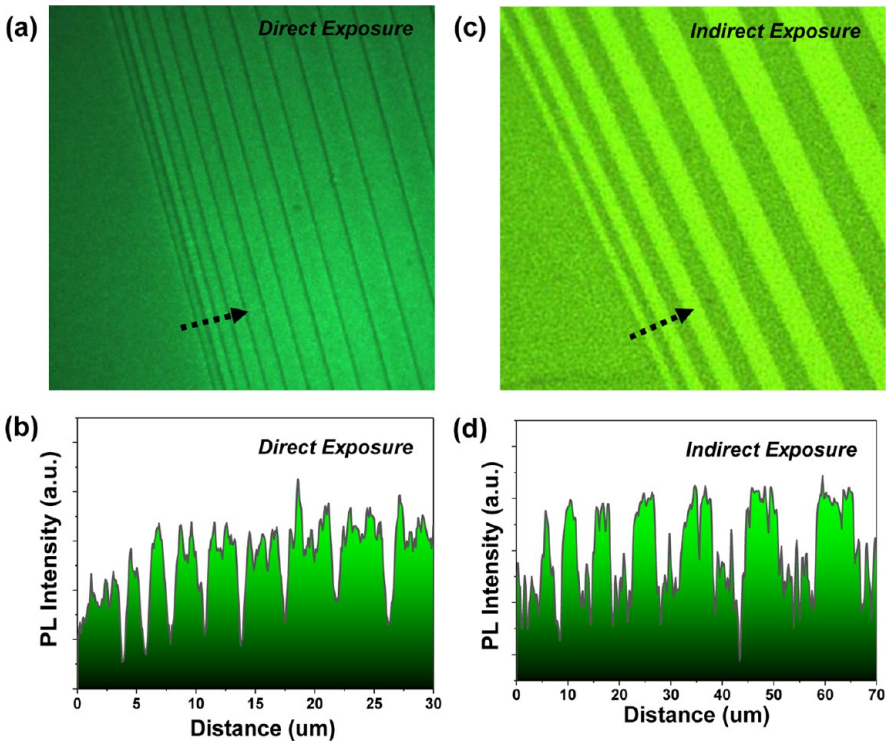

Figure 7. (a) PL image and (b) PL cross-section of photopatterned lines fabricated using the direct exposure approach. (c) PL images and (d) PL cross-section of photopatterned lines fabricated using the indirect exposure approach. Baseline of line-edge profiles corrected for nonuniform light illumination. The black arrows indicate the direction of the PL cross-sections. The direct exposure and indirect exposure photopatterned lines were fabricated using the same PDMS mask.

Large Area Photopatterning (PDMS Mask). The parallel nature of the direct exposure and indirect exposure photopatterning strategies suggests that large film areas can be photopatterned quickly. The results confirm these expectations, with photopatterns being fabricated that successfully span areas up to ~10 mm × 10 mm (Figures S11 and S12). Considered in terms of throughput (patterned area/time), direct exposure patterning offers ~3.3 mm^2/min and indirect exposure ~0.4 mm^2/min. Although we consider these values to be notable, it is difficult to quantitatively compare these values to other studies because throughput is not often quantified in the photopatterning literature. Furthermore, the throughput could be increased by enhancing the intensity of light exposure so these values serve as a general indication of the capabilities offered by these strategies. These photopatterns also have very consistent spatial characteristics over the patterned area (standard deviation ≈ 5%; Figure S13).

High-Resolution/High-Throughput Photopatterning (PDMS Mask). One of the most important advantages of using a patterned PDMS photomask (as opposed to an opaque metal grid) is the potential increase in photopattern resolution. To examine this possibility, a PDMS mask with parallel lines of different width was used to create photopatterns. In this case, both the direct exposure and indirect exposure approaches were implemented (Figure 7a and c, respectively).

PL imaging and cross sections of PL images reveal a number of observations. First, direct exposure patterning can create edge-profile lines with an average fwhm of 630 ± 80 nm and periodicity down to 1.86 ± 0.03 μm (Figure 7b,d). Clearly, this submicron resolution represents a significant improvement in the area of photopatterning because submicron resolution has previously only been possible using a laser exposure source.[23] Additionally, indirect exposure patterning yields high-contrast strips with width of 1.8 ± 0.2 μm.

Second, both direct exposure edge-profile lines and indirect exposure face-profile lines can be patterned with very good resolution without compromising the intensity contrast of the photopattern. Third, these photopatterns correspond closely in size and arrangement to the patterned PDMS photomask used to develop the photopatterns (Figures S3, S14, and S15). Finally, the high resolution afforded by both strategies (submicron for direct exposure and low-micron for indirect exposure) is also accompanied by high-throughput due to the parallel nature of the PDMS patterning mechanism (~0.3−0.6 mm^2/min).

Multiexposure Photopatterning (PDMS Mask). The simplicity of the photopatterning approach and robust nature of the PDMS photomask make multiexposure photopatterning possible. In this case, a photopattern can be created using either the direct or indirect approaches, and then additional photopatterns can be fabricated in the same region.

A number of examples of multiexposure direct exposure and indirect exposure photopatterns are shown in Figure 8. These examples represent only a small fraction of the patterns that can be obtained using this multiexposure approach (Figures S16 and S17).

However, it is clear from the examples that complex and unique photopatterns can be developed that might be difficult (or impossible) to create using other more traditional patterning approaches. Furthermore, multiexposure photopatterning allows for ultradense patterns that can overcome limitations in resolution encountered when using only a single exposure (Figure 8a−c). Finally, multilevel intensity contrast photopatterns are possible in the overlap regions of the

DOI: 10.1021/acs.jpcc.7b03731
J. Phys. Chem. C 2017, 121, 13370−13380

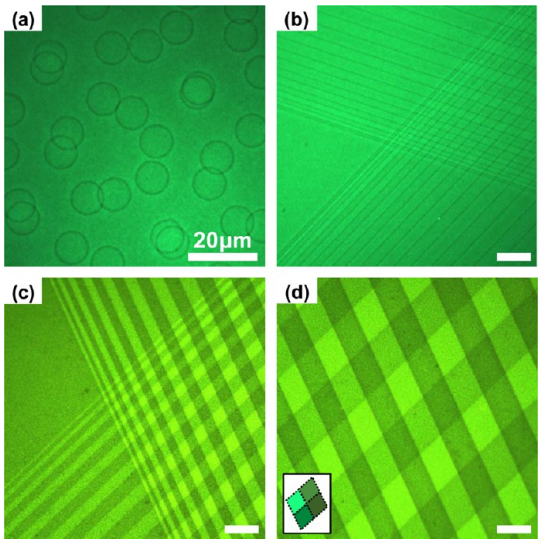

Figure 8. PL images of high-density photopatterns created using multiexposures. Photopattern of multiple exposure "direct exposure" holes (a), multiple exposure "direct exposure" lines (b), and multiexposure "indirect exposure" lines (c, d). (Inset) Schematic of the multilevel intensity contrast present in the cross-hatched patterns (low, medium, high, and very high intensity regions). Scale bar is 20 μm for all images.

photopatterns. For example, Figure 8d clearly shows a four-level contrast system in the cross-hatched region where the photopatterned lines from each exposure step overlap (low, medium, high, very high intensity regions are present (Figure 8d, inset; Figure S17).

Photopatterning via Laser Interference Lithography (Maskless). Laser interference lithography (LIL) is a separate technique where the spatial modulation of light intensity can be provided by the light exposure setup, thereby removing the necessity of having a mask at all. LIL involves exposing a light-sensitive film (QD-polymer in this case) to the interference pattern of multiple laser beams to create the photopattern. An example of photopatterned parallel lines is shown in Figures 9 and S18.

PL imaging shows highly uniform parallel lines with fwhm of ~3 μm, periodicity of ~4.5 μm, and intensity contrast of ~7.5% (Figure 9a; eq S2). A fast Fourier transform (FFT) confirms the highly uniform periodicity of the photopattern (Figure 9a, inset and Figure S19, row 2). Furthermore, lines of submicron fwhm (520 ± 130 nm) and periodicity (800 ± 100 nm) can be created using this technique (Figures 9b and S19). Although the sinusoidal intensity contrast and submicron width make the photopatterned lines more difficult to observe, a FFT of the PL image clearly confirms their presence (Figure 9b, inset).

Figure 9c shows a cross-section of the PL intensity for the lines of ~3 μm fwhm, which follows a near-sinusoidal spatial modulation. A sinusoidal modulation is in accordance with the interference pattern from two coherent beams.[28] As with the photopatterns created using the near-field PDMS photomasks, AFM scanning shows no physical patterning of the QD-polymer film that could account for this PL photopattern, confirming the nonphysical nature of the photopattern (Figure S20).

The LIL patterning approach is also compatible with a multiple-exposure strategy, which can yield a more complex photopattern than that available via a single exposure. Figure 9d

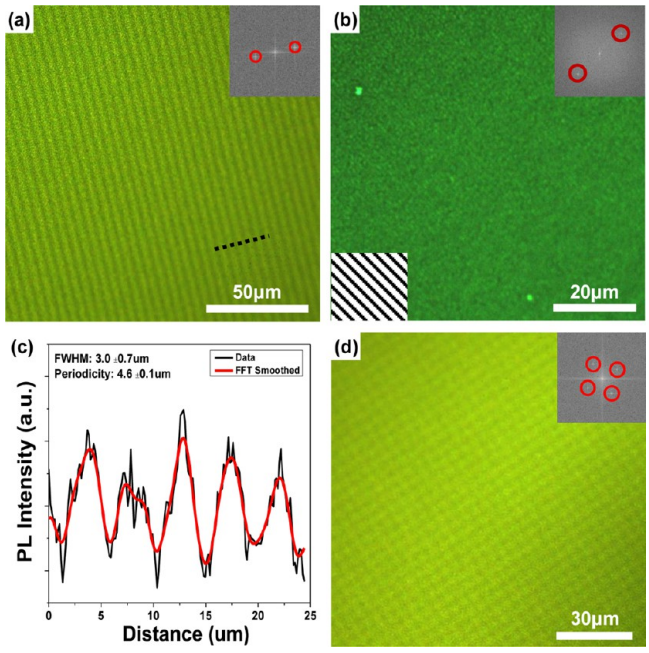

Figure 9. Highly uniform photoluminescence photopatterns created using interference lithography in yellow and green QD-polymer films. PL images of photopatterned parallel lines of fwhm (a) ~3.0 μm (yellow QD film) and (b) ~0.5 μm (green QD film; bottom left inset is a schematic of the line direction). (c) PL cross-section of the ~3 μm fwhm photopatterned lines from (a). (d) Photopattern of cross-hatched lines created by multistep patterning (yellow QD film). Insets are fast Fourier transforms (FFT) of the PL images.

shows a PL image of a dense cross-hatched photopattern created by superposing two sets of lines orthogonal to each other. A FFT of the PL image confirms the cross-hatched sinusoidal periodicity of the entire photopattern (Figure 9d, inset).

Maskless photopatterning using laser interference lithography is also able to create photopatterns over large areas (13 mm × 13 mm) in a short time (within 1 min for this laser power) with exceptional spatial uniformity (fwhm and periodicity). Inspection of the four corners and center of a 13 mm × 13 mm photopattern shows an average periodicity of 5.5 ± 0.5 μm with each region closely matching, which is exceptional, given the lateral areas being considered (Figure S21). In addition to uniformity, this signifies a notable achievement in terms of throughput (~11 mm^2/min) given that this pattern was developed in 15 min. More specifically, it indicates a rate increase up to 1000× compared to previous photopatterning demonstrations.[13,23]

■ CONCLUSIONS

We demonstrate novel photopatterning approaches based on near-field and far-field interference phenomena that yield very high resolution quantum dot photopatterns over exceptionally large areas at exceptionally high throughput. A number of photopatterning routes were outlined that yield either edge-profile or face-profile photopatterns (Table 1). These strategies replace the traditional binary opaque photomask with either near-field or far-field interference phenomena to create the photopattern. The move from a binary photomask to interference-based exposure strategies represents a paradigm shift in the field of photopatterning. Notably, photopatterns fabricated using these interference-based techniques can reach

DOI: 10.1021/acs.jpcc.7b03731
J. Phys. Chem. C 2017, 121, 13370−13380

Table 1. Overview of the Three Outlined Interference-Based Photopatterning Approaches and Their Corresponding Advantages and Disadvantages[a]

approach	mask	photopattern	advantages	disadvantages
direct exposure (near-field)	patterned PDMS (recessed or raised structures)	edge-profile	high resolution (∼500 nm), high intensity contrast, very uniform, fast development	requires π-shift (constraints on photomask and λ_{exp})
indirect exposure (near-field)	patterned PDMS (recessed or raised structures)	face-profile	moderate resolution (∼1.8 μm), high intensity contrast, large-area, very uniform	requires longer development time
laser interference lithography (far-field)	none (2-beam interference)	sinusoidal periodicity	high resolution (∼520 nm), large-area, very uniform, fast development	requires multiple beams for complex patterns, limited intensity contrast for 2-beam interference
scanning-laser (ref 23)	none (direct laser exposure)	line	high resolution (∼575 nm), range of line patterns possible	low-throughput (serial process)
transmission/opaque (ref 15)	high resolution binary mask	face-profile	short development time, simple mask, no interference requirement for λ	resolution ∼7 μm, edge-profile pattern not easily obtained
transmission/opaque (ref 14)	binary mask	face-profile	short development time, simple mask, no interference requirement for λ	resolution >30 μm, edge-profile pattern not easily obtained

[a]The results from notable photopatterning literature references are also provided for comparison (refs 23, 15, and 14). Note, the resolution values quoted correspond to the full-width half-maximum of photopatterned lines or feature width for 2D patterns.

minimum feature sizes of ∼500−1800 nm, which matches the current high resolution offered by direct-write scanning-laser exposure. In addition, these techniques drastically increase the patternable area (cm^2) and throughput (increases of up to 3 orders of magnitude) while maintaining pattern uniformity. These advances address the major constraints associated with resolution and throughput that have traditionally plagued photopatterning (Table 1). Furthermore, photopatterning could have throughput exceeding even common physical patterning techniques like photolithography and electron beam lithography, which require additional process steps to obtain a physical pattern (postbake, development, etch/deposit, strip). Therefore, the developments outlined in this paper could lead to the implementation of photopatterning in place of traditional lithographies if an emissive pattern is required.

Additionally, a single type of photomask is shown to pattern both (novel) edge-profile and (common) face-profile PL emission photopatterns in QD-polymer films by changing the light exposure conditions. Finally, all three approaches can be applied multiple times on the same film area to fabricate ultradense multilevel contrast photopatterns that would be very difficult to obtain using traditional single-exposure strategies. These results highlight an important advance in the area of photopatterning by connecting nano/microscale features to the macroscale sizes that are relevant to many technologies. The simultaneous increase of resolution and throughput offered by these strategies, coupled with their simple and reliable nature, will be critically important for systems that require highly uniform large-area high-resolution photopatterns (e.g., anti-counterfeiting labels and display technologies).

■ ASSOCIATED CONTENT

Supporting Information

The Supporting Information is available free of charge on the ACS Publications website at DOI: 10.1021/acs.jpcc.7b03731.

QD photoluminescence intensity evolution, QD photoluminescence spectra, AFM of QD-polymer films, electromagnetic simulations of light through stamp, photoluminescence microscopy of various high resolution photopatterns, histograms of photopattern feature size/uniformity, equation outlining phase-shift phenomenon in stamp, equation outlining sinusoidal intensity contrast (PDF).

■ AUTHOR INFORMATION

Corresponding Author

*E-mail: vladimir@mse.gatech.edu.

ORCID

Ramathasan Thevamaran: 0000-0001-5058-6167

Zhiqun Lin: 0000-0003-3158-9340

Vladimir V. Tsukruk: 0000-0001-5489-0967

Notes

The authors declare no competing financial interest.

■ ACKNOWLEDGMENTS

Financial support is acknowledged from the Air Force Office of Scientific Research FA9550-14-1-0037 and FA9550-16-1-0187. M.J.S. would like to acknowledge the Science, Mathematics, and Research for Transformation (SMART) scholarship funded by Office of Secretary Defense-Test and Evaluation (OSD-T&E), Defense-Wide/PE0601120D8Z National Defense Education Program (NDEP)/BA-1, Basic Research, SMART Program office Grant Number N00244-09-1-0081. We would like to thank Dong Qin for assisting in the fabrication of the patterned PDMS photomasks and providing the Cr-on-quartz master.

■ REFERENCES

(1) Dang, C.; Lee, J.; Breen, C.; Steckel, J. S.; Coe-Sullivan, S.; Nurmikko, A. Red, green and blue lasing enabled by single-exciton gain in colloidal quantum dot films. *Nat. Nanotechnol.* **2012**, *7*, 335−339.

(2) Gong, X.; Yang, Z.; Walters, G.; Comin, R.; Ning, Z.; Beauregard, E.; Adinolfi, V.; Voznyy, O.; Sargent, E. H. Highly efficient quantum dot near-infrared light-emitting diodes. *Nat. Photonics* **2016**, *10*, 253−257.

(3) Mashford, B. S.; Stevenson, M.; Popovic, Z.; Hamilton, C.; Zhou, Z. Q.; Breen, C.; Steckel, J.; Bulovic, V.; Bawendi, M.; Coe-Sullivan, S.; Kazlas, P. T. High-efficiency quantum-dot light-emitting devices with enhanced charge injection. *Nat. Photonics* **2013**, *7*, 407−412.

(4) Chuang, C.-H. M.; Brown, P. R.; Bulovic, V.; Bawendi, M. G. Improved performance and stability in quantum dot solar cells through band alignment engineering. *Nat. Mater.* **2014**, *13*, 796−801.

(5) Todescato, F.; Fortunati, I.; Gardin, S.; Garbin, E.; Collini, E.; Bozio, R.; Jasieniak, J. J.; Della Giustina, G.; Brusatin, G.; Toffanin, S.; Signorini, R. Soft-Lithographed Up-Converted Distributed Feedback Visible Lasers Based on CdSe-CdZnS-ZnS Quantum Dots. *Adv. Funct. Mater.* **2012**, *22*, 337−344.

DOI: 10.1021/acs.jpcc.7b03731
J. Phys. Chem. C 2017, 121, 13370−13380

(6) Hodaei, H.; Miri, M.-A.; Heinrich, M.; Christodoulides, D. N.; Khajavikhan, M. Parity-time-symmetric microring lasers. *Science* **2014**, *346*, 975−978.
(7) Bozhevolnyi, S. I.; Volkov, V. S.; Devaux, E.; Laluet, J. Y.; Ebbesen, T. W. Channel plasmon subwavelength waveguide components including interferometers and ring resonators. *Nature* **2006**, *440*, 508−511.
(8) Biswas, A.; Bayer, I. S.; Biris, A. S.; Wang, T.; Dervishi, E.; Faupel, F. Advances in top-down and bottom-up surface nanofabrication: Techniques, applications & future prospects. *Adv. Colloid Interface Sci.* **2012**, *170*, 2−27.
(9) Gates, B. D.; Xu, Q. B.; Stewart, M.; Ryan, D.; Willson, C. G.; Whitesides, G. M. New approaches to nanofabrication: Molding, printing, and other techniques. *Chem. Rev.* **2005**, *105*, 1171−1196.
(10) Qin, D.; Xia, Y. N.; Whitesides, G. M. Soft lithography for micro- and nanoscale patterning. *Nat. Protoc.* **2010**, *5*, 491−502.
(11) Young, S. L.; Gupta, M.; Hanske, C.; Fery, A.; Scheibel, T.; Tsukruk, V. V. Utilizing Conformational Changes for Patterning Thin Films of Recombinant Spider Silk Proteins. *Biomacromolecules* **2012**, *13*, 3189−3199.
(12) Whitesides, G. M.; Ostuni, E.; Takayama, S.; Jiang, X. Y.; Ingber, D. E. Soft lithography in biology and biochemistry. *Annu. Rev. Biomed. Eng.* **2001**, *3*, 335−373.
(13) Wang, Y.; Tang, Z. Y.; Correa-Duarte, M. A.; Liz-Marzan, L. M.; Kotov, N. A. Multicolor luminescence patterning by photoactivation of semiconductor nanoparticle films. *J. Am. Chem. Soc.* **2003**, *125*, 2830−2831.
(14) Malak, S. T.; Smith, M. J.; Yoon, Y. J.; Lin, C. H.; Jung, J.; Lin, Z.; Tsukruk, V. V. Programmed Emission Transformations: Negative-to-Positive Patterning Using the Decay-to-Recovery Behavior of Quantum Dots. *Adv. Opt. Mater.* **2017**, *5*, 1600509.
(15) Malak, S. T.; Jung, J.; Yoon, Y. J.; Smith, M. J.; Lin, C. H.; Lin, Z.; Tsukruk, V. V. Large-Area Multicolor Emissive Patterns of Quantum Dot−Polymer Films via Targeted Recovery of Emission Signature. *Adv. Opt. Mater.* **2016**, *4*, 608−619.
(16) Chen, J.; Chan, Y.-H.; Yang, T.; Wark, S. E.; Son, D. H.; Batteas, J. D. Spatially Selective Optical Tuning of Quantum Dot Thin Film Luminescence. *J. Am. Chem. Soc.* **2009**, *131*, 18204−18205.
(17) Gaponik, N.; Hickey, S. G.; Dorfs, D.; Rogach, A. L.; Eychmüller, A. Progress in the Light Emission of Colloidal Semiconductor Nanocrystals. *Small* **2010**, *6*, 1364−1378.
(18) Kapitonov, A. M.; Stupak, A. P.; Gaponenko, S. V.; Petrov, E. P.; Rogach, A. L.; Eychmuller, A. Luminescence properties of thiol-stabilized CdTe nanocrystals. *J. Phys. Chem. B* **1999**, *103*, 10109−10113.
(19) Carey, G. H.; Abdelhady, A. L.; Ning, Z. J.; Thon, S. M.; Bakr, O. M.; Sargent, E. H. Colloidal Quantum Dot Solar Cells. *Chem. Rev.* **2015**, *115*, 12732−12763.
(20) Lin, K. F.; Cheng, H. M.; Hsu, H. C.; Lin, L. J.; Hsieh, W. F. Band gap variation of size-controlled ZnO quantum dots synthesized by sol-gel method. *Chem. Phys. Lett.* **2005**, *409*, 208−211.
(21) Lin, C. H.; Lafalce, E.; Jung, J.; Smith, M. J.; Malak, S. T.; Aryal, S.; Yoon, Y. J.; Zhai, Y.; Lin, Z.; Vardeny, Z. V.; Tsukruk, V. V. Core/Alloyed-Shell Quantum Dot Robust Solid Films with High Optical Gains. *ACS Photonics* **2016**, *3*, 647−658.
(22) Jung, J.; Lin, C. H.; Yoon, Y. J.; Malak, S. T.; Zhai, Y.; Thomas, E. L.; Vardeny, V.; Tsukruk, V. V.; Lin, Z. Crafting Core/Graded Shell−Shell Quantum Dots with Suppressed Re-absorption and Tunable Stokes Shift as High Optical Gain Materials. *Angew. Chem., Int. Ed.* **2016**, *55*, 5071−5075.
(23) Tagliazucchi, M.; Amin, V. A.; Schneebeli, S. T.; Stoddart, J. F.; Weiss, E. A. High-Contrast Photopatterning of Photoluminescence within Quantum Dot Films through Degradation of a Charge-Transfer Quencher. *Adv. Mater.* **2012**, *24*, 3617−3621.
(24) Park, Y.; Felipe, M. J.; Advincula, R. C. Facile Patterning of Hybrid CdSe Nanoparticle Films by Photoinduced Surface Defects. *ACS Appl. Mater. Interfaces* **2011**, *3*, 4363−4369.
(25) Rogers, J. A.; Paul, K. E.; Jackman, R. J.; Whitesides, G. M. Generating similar to 90 nm features using near-field contact-mode photolithography with an elastomeric phase mask. *J. Vac. Sci. Technol., B: Microelectron. Process. Phenom.* **1998**, *16*, 59−68.
(26) Hesjedal, T.; Seidel, W.; Kostial, H.; Yuhas, D. E.; Schneider, S. C. Near-field phase shift photolithography for high-frequency SAW transducers. *Proc. IEEE Ultrasonics Symposium* **2002**, *1-2*, 247−250.
(27) Rogers, J. A.; Paul, K. E.; Jackman, R. J.; Whitesides, G. M. Using an elastomeric phase mask for sub-100 nm photolithography in the optical near field. *Appl. Phys. Lett.* **1997**, *70*, 2658−2660.
(28) Maldovan, M.; Thomas, E. L. *Periodic Materials and Interference Lithography: For Photonics, Phononics, and Mechanics*; Wiley-VCH: Weinheim, Germany, 2008.
(29) Pu, Y.-Y.; Liang, G.-Q.; Mao, W.-D.; Dong, J.-W.; Wang, H.-Z. Fabrication of two-dimensional photonic crystals with triangular rods by single-exposure holographic lithography. *Chin. Phys. Lett.* **2007**, *24*, 983−985.
(30) Jia, L.; Bita, I.; Thomas, E. L. Level Set Photonic Quasicrystals with Phase Parameters. *Adv. Funct. Mater.* **2012**, *22*, 1150−1157.
(31) Liang, G. Q.; Zhu, X. L.; Xu, Y. G.; Li, J.; Yang, S. Holographic Design and Fabrication of Diamond Symmetry Photonic Crystals Via Dual-Beam Quadruple Exposure. *Adv. Mater.* **2010**, *22*, 4524−4529.
(32) Mao, W. D.; Zhong, Y. C.; Dong, J. W.; Wang, H. Z. Crystallography of two-dimensional photonic lattices formed by holography of three noncoplanar beams. *J. Opt. Soc. Am. B* **2005**, *22*, 1085−1091.
(33) Peng, Z. A.; Peng, X. G. Formation of high-quality CdTe, CdSe, and CdS nanocrystals using CdO as precursor. *J. Am. Chem. Soc.* **2001**, *123*, 183−184.
(34) Dabbousi, B. O.; RodriguezViejo, J.; Mikulec, F. V.; Heine, J. R.; Mattoussi, H.; Ober, R.; Jensen, K. F.; Bawendi, M. G. (CdSe)ZnS core-shell quantum dots: Synthesis and characterization of a size series of highly luminescent nanocrystallites. *J. Phys. Chem. B* **1997**, *101*, 9463−9475.
(35) J. A. Woollam Co. Inc. *Guide to Using WVase32, A Short Course in Ellipsometry*; 2010, Chapter 2.
(36) McConney, M. E.; Singamaneni, S.; Tsukruk, V. V. Probing Soft Matter with the Atomic Force Spectroscopy. *Polym. Rev.* **2010**, *50*, 235−286.
(37) Chen, X.; Rogach, A. L.; Talapin, D. V.; Fuchs, H.; Chi, L. Hierarchical Luminescence Patterning Based on Multiscaled Self-Assembly. *J. Am. Chem. Soc.* **2006**, *128*, 9592−9593.

DOI: 10.1021/acs.jpcc.7b03731
J. Phys. Chem. C 2017, 121, 13370−13380